



## Research paper

## A fluorescence-based, gain-of-signal, live cell system to evaluate SARS-CoV-2 main protease inhibition

Rama Dey-Rao<sup>a</sup>, George R. Smith<sup>a</sup>, Uddhav Timilsina<sup>a</sup>, Zackary Falls<sup>b</sup>, Ram Samudrala<sup>b</sup>, Spyridon Stavrou<sup>a</sup>, Thomas Melendy<sup>a,\*</sup>

<sup>a</sup> Department of Microbiology & Immunology, Jacobs School of Medicine & Biomedical Sciences, University at Buffalo, 955 Main St., Buffalo, NY, 14203, USA

<sup>b</sup> Department of Biomedical Informatics, Jacobs School of Medicine and Biomedical Sciences, University at Buffalo, Buffalo, NY, 14203, USA



## ARTICLE INFO

## Keywords:

COVID-19  
SARS-CoV-2  
Protease  
Coronavirus  
Screening  
Antivirals  
Mpro

## ABSTRACT

The likelihood of continued circulation of COVID-19 and its variants, and novel coronaviruses due to future zoonotic transmissions, combined with the current paucity of coronavirus antivirals, emphasize the need for improved screening in developing effective antivirals for the treatment of infection by SARS-CoV-2 (CoV2) and other coronaviruses. Here we report the development of a live-cell based assay for evaluating the intracellular function of the critical, highly-conserved CoV2 target, the Main 3C-like protease (Mpro). This assay is based on expression of native wild-type mature CoV2 Mpro, the function of which is quantitatively evaluated in living cells through cleavage of a biosensor leading to loss of fluorescence. Evaluation does not require cell harvesting, allowing for multiple measurements from the same cells facilitating quantification of Mpro inhibition, as well as recovery of function upon removal of inhibitory drugs. The pan-coronavirus Mpro inhibitor, GC376, was utilized in this assay and effective inhibition of intracellular CoV2 Mpro was found to be consistent with levels required to inhibit CoV2 infection of human lung cells. We demonstrate that GC376 is an effective inhibitor of intracellular CoV2 Mpro at low micromolar levels, while other predicted Mpro inhibitors, bepridil and alverine, are not. Results indicate this system can provide a highly effective high-throughput coronavirus Mpro screening system.

### 1. Background

The current Corona Virus Disease 2019 (COVID-19) is one of the five world-wide pandemics with the highest number of fatalities. COVID-19 is the third zoonotic coronavirus (CoV) pandemic in the last 20 years, suggesting future novel zoonotic CoV outbreaks (Li et al., 2020). Moreover, the wide spread of COVID-19, incomplete protections by vaccinations, and rate of mutation of its causative virus, SARS-CoV-2 (CoV2), have led to predictions that CoV2 is likely to become endemic, and to continue to pose a serious health burden on mankind (Cao et al., 2007; Haseltine, 2020; Lin et al., 2020; Long et al., 2020; Melgaco et al., 2020; Payne et al., 2020; Tang et al., 2011; Wu et al., 2007; Bhopal, 2020). Having effective antivirals against CoV2 will be important for treatment of those who become infected. Moreover, antivirals that target the more conserved viral enzymes are more likely to be effective against future novel CoVs.

Currently, the most effective treatments for COVID-19 are immunomodulators used to treat the cytokine storm resulting from advanced

COVID-19 disease. Antivirals that act directly against CoV2 virus production, by targeting viral-specific enzymes are vitally needed (Archambault and Melendy, 2013; Debing et al., 2015; Neerukonda and Katneni, 2020; Villa et al., 2017). To date, the only FDA-approved antiviral against CoV2 is remdesivir, a repurposed RNA-dependent RNA polymerase (RdRp) inhibitor (Costanzo et al., 2020; de Vries et al., 2020; Durante-Mangoni et al., 2020; Pruijssers et al., 2020; Williamson et al., 2020), that when used alone has limited benefits in treating COVID-19 infections (Ali et al., 2020; Bobrowski et al., 2021; Dong et al., 2021; Giovane et al., 2020; Kalil et al., 2021). More specific antivirals selected/developed against CoV2 are desperately needed. Two viral enzymes often targeted for development of highly effective antiviral agents/treatments are viral genome polymerases (such as the RdRp), and viral-specific proteases required to cleave viral polypeptides into their functional viral proteins (Kausar et al., 2021; Steuber and Hilgenfeld, 2010; Tompa et al., 2021). Some of the most highly effective drug cocktails for HIV treatment and chronic HCV include combinations of viral polymerase and protease inhibitors (Kausar et al., 2021; Steuber

\* Corresponding author.

E-mail address: [TMelendy@buffalo.edu](mailto:TMelendy@buffalo.edu) (T. Melendy).

<https://doi.org/10.1016/j.antiviral.2021.105183>

Received 20 August 2021; Received in revised form 17 September 2021; Accepted 25 September 2021

Available online 7 October 2021

0166-3542/© 2021 The Author(s).

Published by Elsevier B.V. This is an open access article under the CC BY-NC-ND license

(<http://creativecommons.org/licenses/by-nc-nd/4.0/>).

and Hilgenfeld, 2010; Tompa et al., 2021; Kim et al., 2012). While remdesivir alone has shown limited benefit, a combination of remdesivir with a CoV2 protease inhibitor could have far greater effectiveness against COVID-19 (Service, 2021). CoVs encode two viral proteases; the more conserved and arguably the most vital is the CoV 3-chymotrypsin-like Main Protease (Mpro) which is required to generate the majority of mature CoV non-structural proteins including the RdRp subunits (Graham and Baric, 2010). Because Mpro is essential for production of the viral genome replicase our efforts were focused on developing a cell-based drug screening system for this enzyme.

Cell-based assays facilitate drug screening by circumventing issues of drug uptake, intracellular stability and maintenance of function, and toxicity. We report here a cell-based assay that isolates CoV2 Mpro function in human cells in the absence of the other CoV2 proteins. We designed this assay such that inhibition of the Mpro enzyme would result in a positive vital signal, producing a more robust screen with an inherent preliminary counter-screen for cell survival, transcription and protein synthesis. We modified a previously designed red fluorescence protein (RFP) (Alford et al., 2012) biosensor so that cleavage by CoV2 Mpro results in loss of fluorescence. Inhibition of Mpro function allows for synthesis of active, uncleaved RFP, resulting in restoration of fluorescence. This Mpro assay is quantified in living human cells, and can be used to evaluate dose-response of drug activity against CoV2 Mpro, as well as the recovery of Mpro function after drug removal. Our initial results indicate that this assay will be readily adaptable to high-throughput screening.

## 2. Materials and methods

### 2.1. Reagents

GC376 was a kind gift from Dr. David Bruyette at Anivive Life-sciences. Alverine and Bepridil were purchased from Cayman Chemical Company (Ann Arbor, MI). Ebselen was obtained from TCI (Philadelphia, PA). All drugs were stored as 10 mM stock solutions in DMSO at  $-20^{\circ}\text{C}$ . Some antibodies were obtained commercially such as rabbit anti-RFP (Rockland, Philadelphia, PA), rabbit anti-GST (Sigma-Aldrich, St. Louis, MO), rabbit anti-beta Actin ( $\beta$ -ACT  $\sim 40$  kDa) (Abcam, Waltham, MA), used at 1:5000 dilution while Ab-101 for SV40 Large T-antigen (LT  $\sim 94$  kDa), was produced in house from pAB101 hybridoma cell culture and purified on protein A Sepharose (GE) columns. NP40 lysis buffer, Pierce BCA protein assay kit, Halt Protease inhibitor cocktail, 4–20% Novex Tris-glycine gels, Chemiluminescent SuperSignal Western Blot Detection systems, Hoechst 33342 trihydrochloride, Dulbecco's Modified Eagle Media (DMEM), OPTIMEM, fetal bovine serum (FBS) were obtained from Gibco, ThermoFisher Scientific, Grand Island, NY.

### 2.2. Cell lines, cell growth, and imaging

To study the effect of drugs on intracellular expression and function of CoV2 Mpro, adherent AD293 cells (Invitrogen Inc) were cultured in DMEM with 10% (v/v) FBS, at  $37^{\circ}\text{C}$  in 5%  $\text{CO}_2$  atmosphere. OPTIMEM was used for all transfections and treatments with drugs as well as for viewing live cells, using the DMI8 inverted fluorescence microscope (Leica) using a high signal-to-noise YP3 filter cube (Ex532/558; Em570/640) and the DMI8 Thunder Imager software, and the Leica application suite X (LAS X)/Fiji. Quantification reads of the fluorescence in live cells was achieved using the Cytation1 Imaging plate reader (Biotek Instruments Inc., Agilent) with the Gen5 v3.05.11 microplate reader and imaging software. Biosensor fluorescence was measured in kinetic mode using an RFP filter (Ex531/Em593 nm). Calu-3 cells (ATCC HTB-55) were cultured in the same conditions as the HEK293 cells.

### 2.3. DNA plasmids constructed

The CoV2 Mpro expression plasmid, pGST-Mpro, was created by altering the pcDNA3.1+N-GST(Thrombin) expression plasmid (Gene-Script). The amino acid sequence of wild-type (wt) CoV2 Mpro was used to synthesize a codon-optimized open-reading frame and incorporated in frame with the GST open reading frame with the natural N-terminal Mpro amino acid sequence cleavage site such that Mpro cleavage would result in the mature authentic CoV2 Mpro (a cysteine protease with high catalytic efficiency) with native N- and C-termini. Independent mutant expression constructs were created using site-directed mutagenesis (SDM) in the important glutamine at the Mpro N-terminal cleavage site (Q > A), (forward primer: 5'-CGCTGTGCTGGCGAGCGGCTTCAGG-3'; reverse primer: 5'-CCTGAAGCCGCTGCCAGCACAGCG-3') which dramatically decreases the level of Mpro cleavage at the site. The cysteine at the 145th amino acid residue of the mature CoV2 Mpro protein is essential for Mpro activity and was mutated to an alanine (forward primer: 5'-CTGAACGGCTCCGCTGGCAGCGTGG-3'; reverse primer: 5'-CCACGCTGCCAGCGGAGCCGTTCA-3').

The parent plasmid, pRFP1B1-DEVD was purchased from Addgene Inc, and altered such that caspase 3 cleavage sequence between the two domains of RFP, DEVDG, was changed to AVLQS, a strong consensus site for cleavage by Mpro. SDM was used to create a Q > A mutation in the AVLQS Mpro cleavage site which dramatically decreases the efficiency of cleavage (forward primer 5'-GCCGTGTGGCGAGCGGAGCCAC-3'; reverse primer 5'-GTGGCTCCGCTGCCAGCACGGC-3').

### 2.4. Extract preparation and immunoblotting

Total protein from untransfected or transfected HEK293T or AD293 cells that were either mock (DMSO) treated or treated with drugs/recovered, were resolved by SDS PAGE followed by immunoblotting. Cell lysates were prepared using NP40 lysis buffer (containing 1% NP40, 250 mM NaCl, 50 mM Tris-Cl (pH 7.4) with PMSF and protease inhibitors on ice, subjected to centrifugation in a microfuge for 15 min at  $4^{\circ}\text{C}$  at 15,900 RCF. Protein levels were standardized using BCA protein assay, flash frozen in liquid nitrogen and stored at  $-80^{\circ}\text{C}$ . Total cellular protein ( $\sim 20$ – $30$   $\mu\text{g}$  per lane) were resolved using 4–20% Tris-glycine PAGE and blotted on to nitrocellulose membranes (via iBlot 2 gel transfer using transfer template program P0) following standard procedures. Anti-GST, RFP and LT primary antibodies (1:1000) and HRP-linked secondary antibody (1:10,000) were diluted in 5% non-fat dry milk in Tris-buffered saline + 0.1% Triton X-100 (TBST, pH 7.5). Blots were washed with TBST alone. Chemiluminescent detection was performed and image of immunoreactive bands were captured using a ChemiDoc MP (Bio-Rad, Hercules, CA). The relative optical densities of the digitized images were quantified using Fiji (an update of ImageJ by NIH).

### 2.5. Microscopy and BioTek cytation 1 quantification

A total of 150,000 or 50,000 AD293 cells were seeded in 24-well and 96-well plates, respectively, and maintained in a humidified tissue culture incubator at  $37^{\circ}\text{C}$  in a 5%  $\text{CO}_2$  atmosphere to 80–90% confluency. Triplicate wells were either left untransfected or were transfected in serum free OPTIMEM, using Lipofectamine 2000 with indicated vector constructs. After 21 h, cells were stained with 0.5  $\mu\text{g}/\text{ml}$  cell-permeant Hoechst 33342 in prewarmed OPTIMEM and treated with either DMSO alone or varying concentrations of drugs (e.g., GC-376, Bepridil, Alverine or Ebselen). Plates with live cells were maintained at  $37^{\circ}\text{C}$  in 5%  $\text{CO}_2$  in the imaging chamber of the Cytation 1 Imaging Reader; a DAPI filter (Ex377/Em447nm) in channel 1 was used to monitor Hoechst/DNA (blue fluorescence) and to allow for precise instrument autofocusing from well-to-well, and RFP filter (Ex531/Em593 nm) in channel 2 to measure the presence of the biosensor (red fluorescence) in kinetic mode. Measurements were monitored every hour for 15–20 h.

Three such experiments were evaluated, each with triplicate samples, followed by MTT cell viability determination. In additional experiments, cells were further monitored for 23 h after removing GC376 at the 17th hour and adding OPTIMEM for 23 h recovery; also evaluating cell viability using the MTT assay. Inhibition dose response curves were established and IC<sub>50</sub> calculated using Quest Graph™ EC50 Calculator (<https://www.aatbio.com/to>).

Photomicrographs were also obtained of transfected living cells with or without drugs in OPTIMEM, and visualized using a 10X objective on a Leica DMI8 inverted fluorescence microscope. Phase contrast and fluorescent images were acquired simultaneously using Thunder Imager software. All images were acquired using identical imaging parameters and were visualized using LasX/Fiji software (Leica/NIH).

### 2.6. MTT assay

Cell viability was measured using the MTT (3-(4,5-dimethylthiazol-2-yl)-2,5-diphenylterazolium bromide) tetrazolium reduction assay (Riss et al., 2004). Briefly, MTT reagent (0.5 mg/ml final concentration) was added to the HEK 293 or 293T cells treated with GC376 either after the kinetic reads or after recovery. Formazan crystals produced by viable cells were solubilized with a solution of 40% dimethylformamide, 16% sodium dodecyl sulfate and 2% glacial acetic acid (pH 4.7) and the absorbance was measured at 570 nm using a Versamax tunable microplate reader and Softmaxpro software version 5.4 (MDS Analytical Technologies, San Jose, CA, USA).

### 2.7. SARS-CoV-2 (CoV2) infections and RNA detection

Calu-3 cells were seeded at a density of  $0.1 \times 10^6$ /well in a 24-well plate. 48 h later, cells were infected with CoV2 virus (2019-nCoV/USA-WA1/2020; 0.01 MOI) and cultured in the presence of DMEM containing DMSO or different concentrations of the drug GC 376 for 24 h using appropriate safety measures for CoV2 live virus manipulations (BSL-3 facility at the University at Buffalo). RNA was isolated using RNeasy kit (Qiagen). cDNA was synthesized using the SuperScript III First Strand Synthesis kit (Invitrogen). RT-qPCR was performed using the PowerUp SYBR Green PCR master mix kit (Applied Biosystems). CFX384 Touch Real-Time PCR detection system (Bio-Rad) was used for the RT-qPCR

amplifications. The reactions were performed under the following conditions: 50 °C for 2 min, 95 °C for 2 min, followed by 40 cycles of 95 °C for 15 s and 60 °C for 1 min, followed by a dissociation protocol. The primers used for CoV2 Spike detection are 5'- CCTACTAAATTAATGATCTCTGCTTTACT-3' and 5'-CAAGCTATAACGCAGCCTGTA-3', while hGAPDH primers 5'-AACGGGAAGCTTGTATCAATGGAAA-3' and 5'-GCATCAGCAGAGGGGGCAGAG-3' were used for normalization. The relative amplification for each sample was quantified from standard curves generated using known quantities of DNA standard templates. CoV2 RNA copy numbers were normalized to hGAPDH for DMSO-treated conditions and were set as 100% to calculate the relative CoV2 Spike RNA levels.

## 3. Results

### 3.1. Intracellular production of mature wild-type CoV2 Mpro

Mpro is one of the CoV proteins produced by proteolytic cleavage of the large polyproteins (ORF1a/b) directly translated from the incoming viral genomic RNA (Graham and Baric, 2010). The enzymatic activity of CoV2 Mpro has been shown to be adversely affected by additional amino acid residues to both the N- and C-termini, where even a few amino acid residues can result in 5- to 20-fold inhibition of enzymatic function (shown for SARS-CoV Mpro, >96% identical to CoV2 Mpro) (Xue et al., 2007). The fully functional Mpro with the native N-terminal Mpro cleavage site was expressed as a GST-fusion protein, such that Mpro cleavage would produce the wild-type mature Mpro protein (Fig. 1A). When this CoV2 GST-Mpro expression vector was transfected into HEK 293T cells, immunoblotting revealed only a ~27 kDa GST signal (Fig. 1B, lane 2, GST). without any GST-Mpro fusion protein as was previously demonstrated for SARS-CoV GST-Mpro expressed in *E. coli* (Xue et al., 2007). When the critical glutamine in the N-terminal cleavage site was mutated to an alanine, (known to substantially inhibit Mpro cleavage (Xue et al., 2007; Chuck et al., 2010; Wu et al., 2015)), it resulted in a dramatic increase of the uncleaved GST-Mpro fusion protein (~61 kDa), but low levels of cleaved GST were still produced (Fig. 1B, lane 3), consistent with findings for other CoV Mpro enzymes (Xue et al., 2007; Chuck et al., 2010; Wu et al., 2015). When C145, (critical for Mpro's catalytic function (Jin et al., 2020)), was mutated to

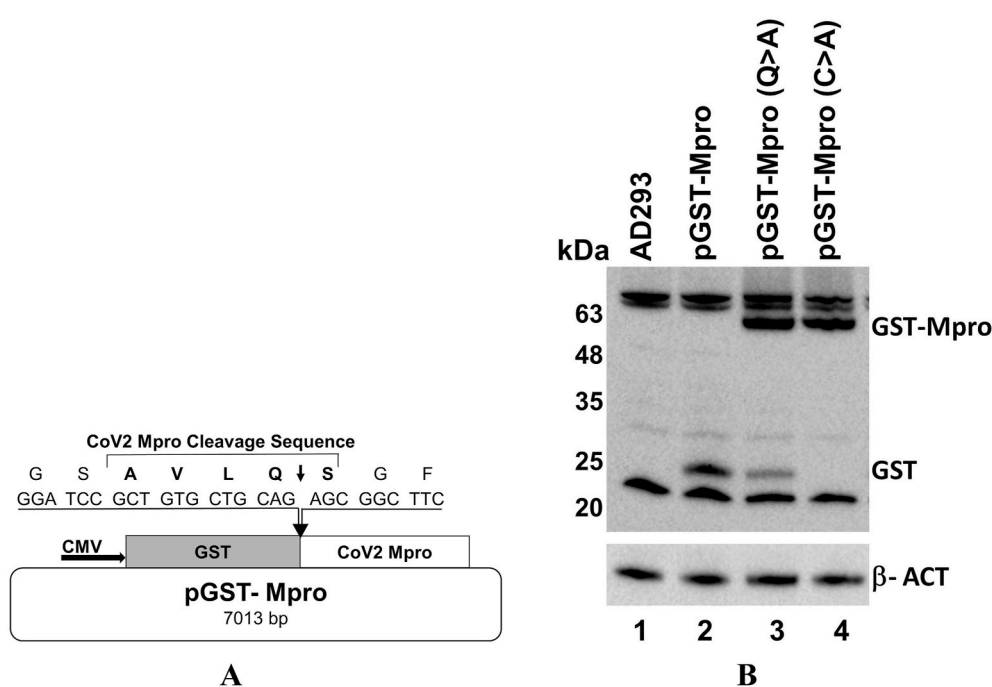


**Fig. 1.** Expression of wt functional CoV2 Mpro: A) Graphic depiction of the pGST-Mpro vector (pcDNA3.1-GST-CV2-3CL), indicating that codon-optimized CoV2 Mpro is expressed from the CMV promoter as a fusion protein with GST incorporating the natural Mpro cleavage site between GST and Mpro. Cleavage at the site will produce the natural N-terminus of fully mature cleaved CoV2 Mpro. B) Immunoblotting of AD293 cells (lane 1) transfected with the pGST-Mpro vector (lane 2), or with the pGST-Mpro vector with mutations in the Mpro cleavage site (lane 3) or in the catalytic site of Mpro (lane 4), for GST (upper panel) or for beta actin ( $\beta$ -ACT, ~40 kDa, lower panel) as loading control.

alanine (C145A) predictably the enzyme was inactive and unable to cleave the AVLQS sequence, resulting in the GST-Mpro fusion protein, and no cleaved GST (Fig. 1B, lane 4). Together, these results demonstrate that the pGST-Mpro vector when expressed in HEK293 cells produces a CoV2 GST-Mpro fusion protein that self-cleaves to GST and the mature, fully functional wild-type Mpro.

### 3.2. Expression of an RFP biosensor for monitoring Mpro function

The biosensor for detection and quantification of CoV2 Mpro function was based on adaptation of a previously developed dimerization-dependent RFP with the interaction mutationally weakened, with a caspase 3 cleavage site engineered between the two domains in a fusion protein construct, such that caspase 3 cleavage results in loss of RFP fluorescence (Alford et al., 2012; Mitchell et al., 2018). This vector was altered changing the DEVDG caspase 3 cleavage site to AVLQS, a sequence chosen based on its high conservation among cleavage sites for all CoV Mpros (Fig. 2A), identified by compiling the 77 CoV Mpro

cleavage sites of all circulating human, SARS, and MERS CoV sequences (Crooks et al., 2004) (Supplemental Fig. 1). The AVLQS sequence has also been shown to be efficiently cleaved *in vitro* by various recombinant CoV Mpros, including CoV2 Mpro (Xue et al., 2007; Chuck et al., 2010; Jin et al., 2020; Muramatsu et al., 2016). When either the parental, or the pRFP-AVLQS vector (Fig. 2B) were transfected into HEK293T cells, each produced the predicted (~54 kDa) RFP protein, as well as lower levels of a lightly smaller breakdown product (~40 kDa) (Fig. 2C) (Alford et al., 2012; Mitchell et al., 2018). Both vectors also produced similar levels of fluorescence (Fig. 2D, panels 4 and 6).

### 3.3. Intracellular cleavage of RFP biosensor by CoV2 Mpro

Co-expression of the RFP-AVLQS biosensor with Mpro was predicted to result in cleavage of the biosensor, separation of the two RFP domains, resulting in reduction of RFP fluorescence (Fig. 3A). Co-transfection of these two expression vectors and immunoblotting for RFP confirmed that expression of wt Mpro cleaved the majority of the

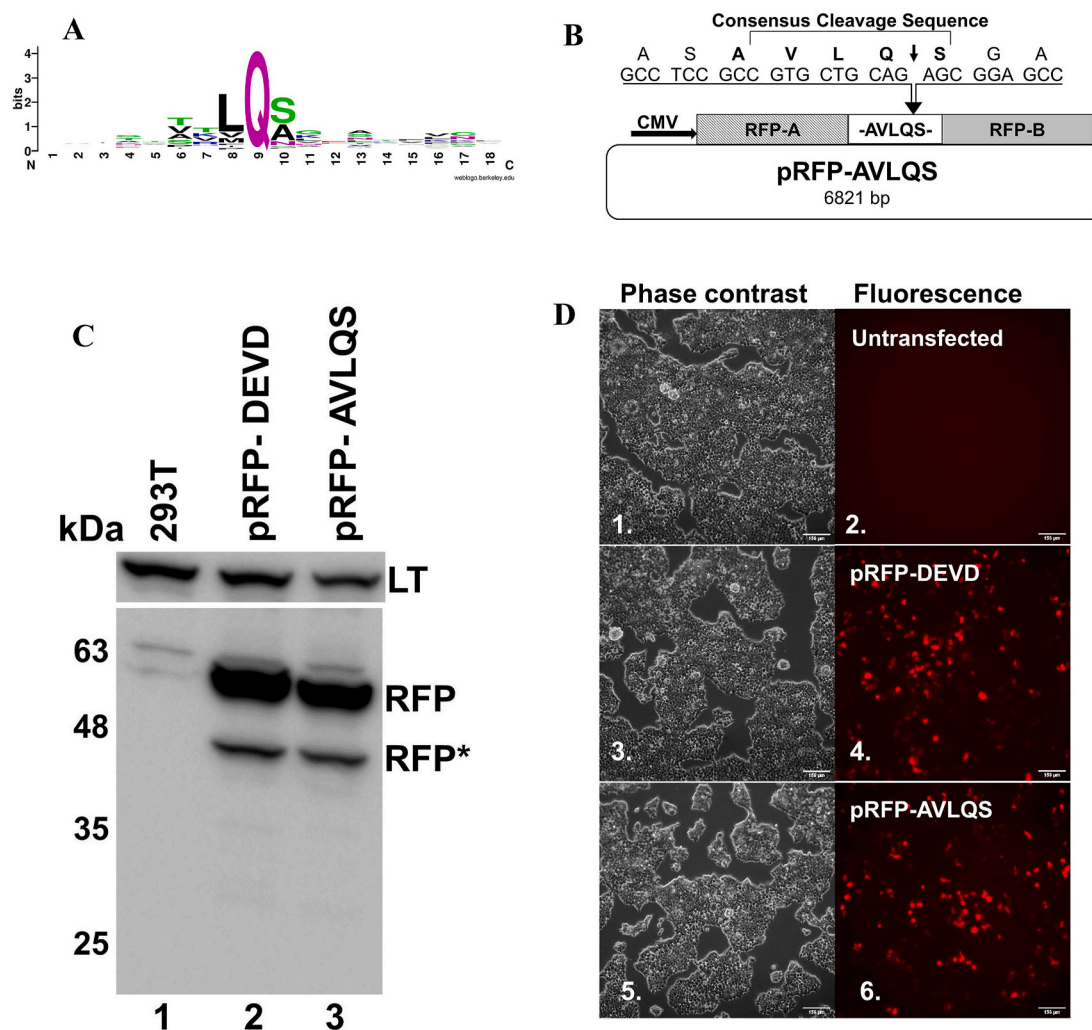


**Fig. 2.** Creation and expression of an RFP biosensor to detect CoV2 Mpro function: A) The consensus sequence for cleavage by Mpro, was computed using WebLogo version 3.0 using 77 cleavage sites, 11 each from SARS-CoV, MERS-CoV, SARS-CoV2, HCoV-229E, HCoV-NL63, HCoV-OC43 and HCoV-HKU1 (Supplemental Fig. 1). B) Graphic depiction of the pRFP-AVLQS vector, indicating the AVLQS cleavage site that was incorporated between the two RFP domains required to be tethered to allow for association and fluorescence. Expression of the RFP fusion protein is driven by the CMV promoter. C) Immunoblotting of HEK-293T cells untransfected (lane 1) or transfected with either the parental pRFP-A1B1-DEVD vector (lane 2), or the pRFP-AVLQS vector (lane 3), for RFP (lower panel), or for SV40 Large T-antigen (LT, ~94 kDa, upper panel) as a loading control. The heavy top band is the fluorescent RFP protein (RFP, ~54 kDa) and the lower lighter band represents a breakdown product that is naturally produced upon expression in human cells (~40 kDa RFP\*) D) Phase contrast (odd) and fluorescence (even) images captured simultaneously using inverted microscopy demonstrate non-fluorescent untransfected cells (Cao et al., 2007), and similar levels of RFP fluorescence in cells transfected with either pRFP-A1B1-DEVD or pRFP-AVLQS (compare 4 vs 6). Bar = 156  $\mu$ m.

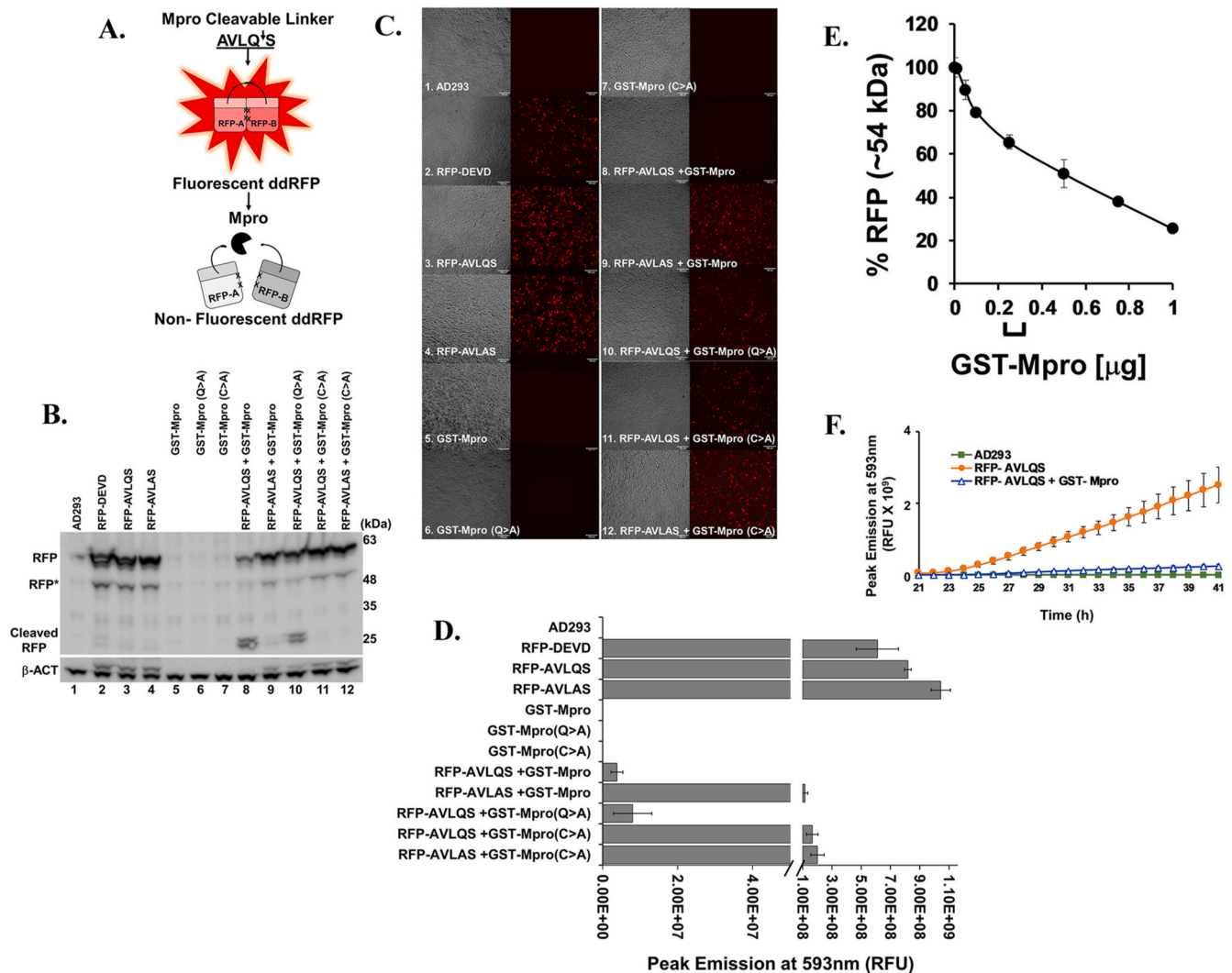


**Fig. 3.** Co-expression with CoV2 Mpro produces intracellular cleavage of the RFP biosensor. A) Graphic diagram of the RFP biosensor depicting two domains of RFP that had previously been mutated to weaken the interaction such that the two domains must be tethered as a single polypeptide (54 kDa) to allow domain dimerization to fluoresce (top). Upon Mpro cleavage of the AVLQS amino acid sequence, the two RFP domains (~27 kDa) dissociate, and fluorescence is lost (lower). B) Immunoblotting: of untransfected AD293 cells (lane 1) and cells transfected with either: the parental pRFPΔ1B1-DEVD vector (lane 2), or the wt pRFP-AVLQS vector (lane 3), with the Q of AVLQS mutated to A (pRFP-AVLAS, lane 4), pGST-Mpro (wt) (lane 5), pGST-Mpro with Q to A mutation in the N-terminal cleavage site (lane 6), pGST-Mpro with the catalytic C145 mutated to A (lane 7). Dual transfections were carried out with the following combinations: pRFP-AVLQS (wt) with pGST-Mpro (wt) (lane 8), pRFP-AVLAS with pGST-Mpro (wt) (lane 9), pRFP-AVLQS (wt) with pGST-Mpro (Q > A) (lane 10), pRFP-AVLQS (wt) with pGST-Mpro (C > A) (lane 11), and pRFP-AVLAS with pGST-Mpro (C > A) (lane 12). All were immunoblotted for RFP (upper panel) and for β-ACT (lower panel) as a loading control. (The same extracts immunoblotted for GST to analyze Mpro expression and cleavage are shown in Supplemental Fig. 2.) C) Microscopy: The same transfections as in B were visualized using phase contrast and fluorescence microscopy, as indicated (same numbering as Fig. 3B). Bar = 156 μm. D) Quantification of the RFP fluorescence of the panels in Fig. 3C using the BioTek Cytation 1 as described in the Methods. E) Determination of effective pGST-Mpro:pRFP-AVLQS ratios: The Fiji software suite was used to quantify the signals of RFP immunoblots in HEK293T cells transfected with 1 μg pRFP-AVLQS and the indicated levels of pGST-Mpro. The intensity of the 54 kDa RFP band, normalized to LT, provided a measure of RFP levels, compared to the RFP 54 kDa level in cells transfected with pRFP-AVLQS alone set as 100%. Relative RFP levels in the cells co-transfected with varying amounts (1–0.005 μg) of pGST-Mpro established that ratios of ~1:4 pGST-Mpro to pRFP-AVLQS resulted in near linear changes in RFP intensity with changing Mpro levels, while still retaining sufficient RFP levels to readily detect fluorescence (also see Supplemental Fig. 3). A representative immunoblot used to generate this graph is shown in Supplemental Fig. 3A. Microscopy verifying these plasmid levels produce readily detectable levels of fluorescence is shown in Supplemental Fig. 3B. F) Time course of fluorescence: AD293 cells were either untransfected (squares), or transfected with pRFP-AVLQS (circles) or co-transfected with pGST-Mpro and pRFP-AVLQS (triangles) in the ratio of 1:4 for 21 h. The fluorescence output of live cells was monitored for Hoechst-DNA (blue) and biosensor expression (red), every hour for 20 h following the media exchange as described in Methods. (Micrographs at the 36th hour are shown in Supplemental Fig. 4).

RFP-AVLQS, producing the predicted ~27 kDa cleavage products (Fig. 3B, compare lanes 3 and 8) and dramatically decreasing RFP fluorescence (Fig. 3C, panels 3 and 8). This cleavage was dependent upon the activity of Mpro, as the C145A catalytically dead Mpro resulted in no cleavage (Fig. 3B, lane 11), and fluorescence was not eliminated (Fig. 3C, panel 11 compared to panels 8 and 3). As with the GST-CoV2 Mpro fusion itself, mutation of the key glutamine residue in the

cleavage site of Mpro to alanine resulted in decreased cleavage of the RFP biosensor (Fig. 3B, lane 10), and by increased fluorescence as compared to wt Mpro (Fig. 3C, compare panels 10 and 8). This inhibition occurred even though the catalytic domain of Mpro was not mutated (Fig. 3B,C compare lanes and panels, 10, to 3 and 8), consistent with previous reports about decreased Mpro activity when additional amino acids are on the N-terminus (Xue et al., 2007). Mutating the glutamine in

the RFP cleavage site and co-transfecting with wt Mpro showed an even greater decrease in RFP cleavage (Fig. 3B, lane 9), and higher fluorescence levels (Fig. 3C compare panel 9 to panel 10). (Immunoblotting of these same samples for GST, confirming cleavage of the GST-Mpro fusion protein consistent with Mpro activity, is shown in Supplemental Fig. 2) Quantification of the fluorescence in all the panels of Fig. 3C is shown in Fig. 3D.

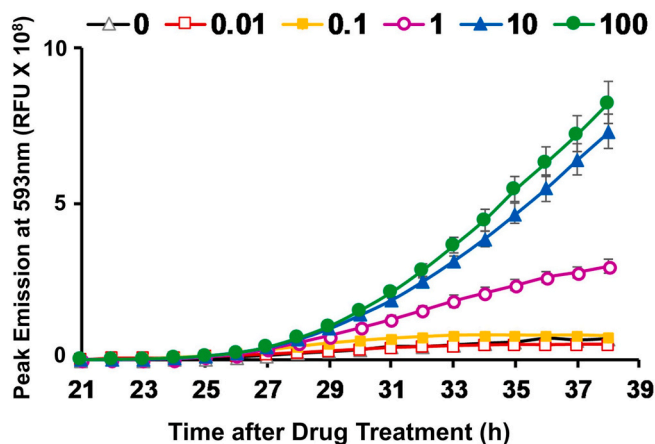
It is important to recognize that the RFP fluorescence is not merely positive or negative, but can be detected at varying levels that can be quantified. The two plasmids (Figs. 1A and 2B) in these assays were used at a ratio of 1:4 of (pGST-Mpro/pRFP-AVLQS). By quantifying levels of RFP 54 kDa from a fixed level of pRFP-AVLQS, using varying levels of pGST-Mpro, we establish plasmid levels where changes in pGST-Mpro have a substantial effect on RFP levels, while retaining readily detectable fluorescence – the approximate “linear range” of the assay (Fig. 3E, Supplemental Fig. 3A and 3B). This was done to optimize the sensitivity of the assay.

To optimize time, live cells transfected with pRFP-AVLQS, with or without Mpro, were monitored hourly for RFP, normalizing for the stable Hoechst signal (Supplemental Fig. 4 and data not shown). The RFP fluorescence signal was dramatically and measurably reduced in the presence of Mpro from hour 25 throughout the 41 h time course

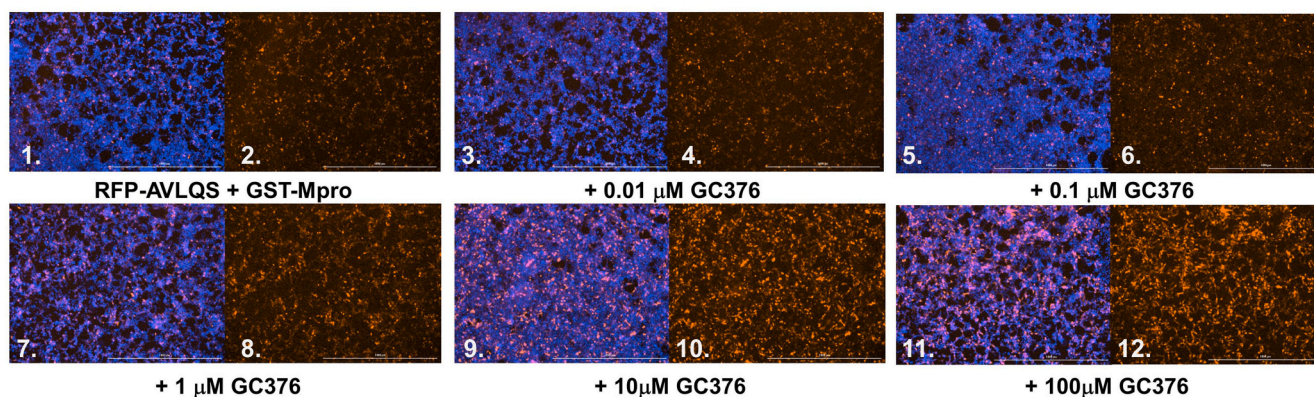
(Fig. 3F). The consistency of the fluorescence signal ratios over most of the 20 h time frame and the ability to obtain multiple measurements from a single well demonstrate the great advantage of using this live cell readout assay.

#### 3.4. Use of the expression vectors to evaluate inhibition of CoV2 Mpro function intracellularly

To determine whether this system could be used for evaluating inhibition of CoV2 Mpro function we utilized GC376, an investigational drug in trials for feline coronavirus that has been shown to be effective at inhibiting CoV2 Mpro (Fu et al., 2020; Ma et al., 2020a; Vuong et al., 2020). Cells expressing the RFP-AVLQS biosensor and CoV2 Mpro (resulting in cleavage of the RFP-AVLQS and low fluorescence, as in Fig. 3C panel 8) were treated with ten-fold dilutions of GC376, from 100 to 0.01  $\mu\text{M}$ . Previously synthesized, Mpro-cleaved RFP cannot reconstitute RFP fluorescence, but if Mpro is inhibited then newly synthesized RFP-AVLQS would remain uncleaved, so reconstitution of fluorescence over time would be anticipated. An advantage of this live cell-based system is that harvesting is not required, allowing kinetic assessment of recovery of fluorescence for all drug levels over the entire 17 h drug treatment phase (Fig. 4A). Treatment of the RFP-AVLQS- and



A



B

**Fig. 4.** GC376 Inhibition of intra-cellular CoV2 Mpro: A) AD293 cells were co-transfected with pGST-Mpro and pRFP-AVLQS (ratio of 1:4) for 21 h. Cells stained with Hoechst were treated with varying levels of GC376: 0  $\mu\text{M}$  (open triangles), 0.01  $\mu\text{M}$  (open squares), 0.1  $\mu\text{M}$  (filled squares), 1  $\mu\text{M}$  (open circles), 10  $\mu\text{M}$  (filled triangles), and 100  $\mu\text{M}$  (filled circles). The fluorescence output of the live cells was monitored as in Fig. 3F for Hoechst-DNA and RFP every hour for 17 h following addition of GC376. Inhibition of Mpro by GC376 is indicated by increasing levels of fluorescence (note the greater sensitivity of the scale in Fig. 4A as compared to Fig. 3F). B) Images shown are from hour 36, or 15 h after addition of drug/OPTIMEM), visualizing for RFP (even panels) or RFP and DNA (odd panels), using the Cytation 1 imaging reader as described above. Bar = 1000  $\mu\text{m}$ .

Mpro-expressing cells with 0.01 or 0.1  $\mu\text{M}$  GC376 showed little difference from mock-treated cells (Fig. 4A, open boxes, filled boxes and open triangles); and microscopically at hour 36, Fig. 4B panels 2, 4, 6). However, treatment with 1  $\mu\text{M}$  GC376 showed clearly detectable recovery of RFP fluorescence levels (Fig. 4A open circles, Fig. 4B panel 8), and treatment with 10 and 100  $\mu\text{M}$  GC376 showed high levels of RFP fluorescence recovery (Fig. 4A filled triangles and filled circles, and 4B panels 10 and 12). Since inhibition of Mpro is determined by expression of new RFP-AVLQS, this indicates that these drug levels are not toxic; nonetheless cell viability was confirmed at all levels of GC376 (0.01–100  $\mu\text{M}$ ) (Fig. 5A, triangles).

### 3.5. Levels of GC376 required to inhibit intracellular Mpro are consistent with those required to inhibit CoV2 infection of human lung cells

To quantify the inhibition of intracellular CoV2 Mpro by GC376, the 36 h time point values (Fig. 4A) from three experiments ( $n = 9$ ) were plotted on a semi-logarithmic graph to establish the half-maximal inhibitory concentration value. The concentration of GC376 calculated to show 50% inhibition of Mpro after 15 h of drug treatment was  $2.71 \pm 0.52 \mu\text{M}$  (<https://www.aatbio.com/to>) (Fig. 5A). To evaluate whether the observed levels of GC376 required to inhibit intracellular CoV2 Mpro were consistent with levels required to inhibit infection by CoV2 virus we infected Calu-3 human lung epithelial cells with CoV2 at a multiplicity of infection (MOI) of 0.01, before applying the same five concentrations of GC376 tested above, and evaluating virus production using RT-qPCR of CoV2 RNA versus cellular GAPDH. Viral RNA was reduced by GC376 treatment in a dose-dependent manner (Fig. 5B). The  $\text{IC}_{50}$  of GC376 for the viral infection ( $0.59 \pm 0.07 \mu\text{M}$ ) was close to levels required to inhibit intracellular CoV2 Mpro in our human cell-based assay; both assays showed dose-dependence, and GC376 levels required for inhibition were also consistent with published  $\text{EC}_{50}$  values for GC376 for purified CoV2 Mpro (Fu et al., 2020; Ma et al., 2020a; Vuong et al., 2020; Li and Kang, 2020; Hu et al., 2021).

### 3.6. Use of the cell-based CoV2 Mpro biosensor assay in evaluating other predicted Mpro inhibitors

CoV2 Mpro is an excellent target for CoV2 antivirals; hence, much effort has been directed at identifying and testing existing drugs that

could be repurposed for use against Mpro for the COVID-19 pandemic (Jin et al., 2020; Fu et al., 2020; Ma et al., 2020a; Li and Kang, 2020; Drayman et al., 2020; McKee et al., 2020; Pillaiyar et al., 2016; Rathnayake et al., 2020; Vatansever et al., 2020; Zhu et al., 2020). However, these approaches rarely demonstrate that these drugs will inhibit Mpro function in living cells. The assay above was used to evaluate two of the drugs from the panel of FDA-approved drugs and bioactive compounds that we previously predicted to target CoV2 Mpro with some of the highest predicted affinities (Mangione et al., 2020). One of these drugs, Bepridil, has been shown to inhibit purified CoV2 Mpro *in vitro* (Vatansever et al., 2021). Using the computational drug-protein interaction program, CANDOCK (Chopra et al., 2016; Fine et al., 2020), these two drugs, Alverine and Bepridil, as well as GC376 were docked onto the CoV2 Mpro structure (Zhang et al., 2020). Each drug was predicted to bind CoV2 Mpro, and each docked into the active site pocket of the enzyme, that contains a highly nucleophilic catalytic cysteine residue (Vatansever et al., 2021), with predicted relative binding scores of  $-69.4$ ,  $-71.3$ , and  $-93.4$ , respectively (Fig. 6A). Using this assay, we tested the ability of these drugs to inhibit intracellular CoV2 Mpro function; the drugs were evaluated at high, but non-toxic drug levels (100  $\mu\text{M}$ ), every hour over an 18 h time course (Fig. 6B). Bepridil showed no inhibition of intracellular CoV2 Mpro activity as compared to GC376, which resulted in a dramatic increase in fluorescence levels between hours 8 and 18 (Fig. 6B, compare triangles to circles). Alverine, which was suggested to potentially inhibit CoV2 Mpro based on predicted structural interaction alone (Mangione et al., 2020), exhibited a slight increase in basal fluorescence immediately upon treatment of the transfected cells, but no time-dependent increase in RFP fluorescence over the course of the treatment (Fig. 6B boxes). We concluded that Bepridil and Alverine were ineffective at inhibiting CoV2 Mpro intracellularly at 100  $\mu\text{M}$  levels within 18 h of treatment, a time by which treatment with GC376 had a profound effect on Mpro activity (Fig. 6B; lack of fluorescence at 18 h also shown in micrographs in Supplemental Fig. 5A). The fact that two of the FDA compounds predicted to have the highest affinity for Mpro (Mangione et al., 2020), are predicted to have lower affinity than GC376 (Fig. 6A), and to not be effective in inhibiting intracellular Mpro (Fig. 6B), suggests that effective COVID-19 drugs that target Mpro are not likely to be found by repurposing existing FDA-approved drugs. Similarly, it was found that Ebselen, which has also been reported to inhibit purified CoV2 Mpro (Ma et al., 2020b; Sun

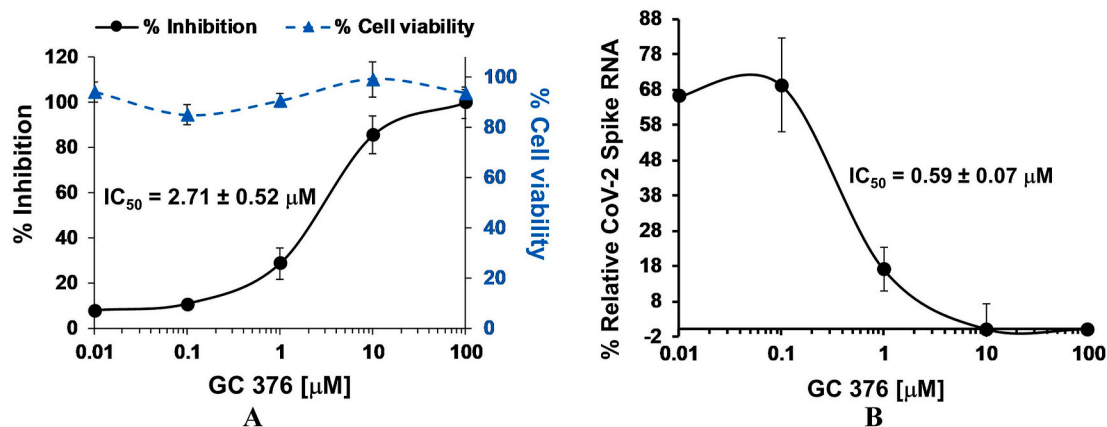


**Fig. 5.** GC376 inhibits intracellular CoV2 Mpro and CoV2 infection of human lung cells at similar levels: A) Dose-response curves of the time courses of GC376 dilutions (Fig. 4) were carried out. For each experiment fluorescence values at the 15th hour of drug treatment were expressed as a percentage compared to 100  $\mu\text{M}$  GC376. Data (black circles) are shown as means ( $\pm$  SEM) from three separate experiments with a nonlinear fit curve (total  $n = 9$ ). The  $\text{IC}_{50}$  was determined to be  $2.71 \pm 0.52 \mu\text{M}$  using a web-based calculator (<https://www.aatbio.com/to>). Cell viability at each level of GC376 relative to vehicle only (DMSO) ( $\pm$ SEM) is shown (triangles). B) Calu-3 human lung epithelial cells were infected with CoV2 virus at a multiplicity of infection (MOI) of 0.01 before applying the Mpro inhibitor, GC376, at the same levels as above: (100–0.01  $\mu\text{M}$ ). Cells were harvested 24 h post-infection, RNA was collected and used to perform reverse transcription (RT)-qPCR using CoV2- and hGAPDH- (a cellular control gene) specific primers to detect relative amounts of CoV2 RNA. The CoV2 RNA copy number was normalized, setting hGAPDH in DMSO-only conditions to 100%, to determine the relative CoV2 Spike RNA levels at the various GC376 concentrations. Results are shown as the mean ( $n = 3$ ,  $\pm$  SEM) with a nonlinear fit curve.

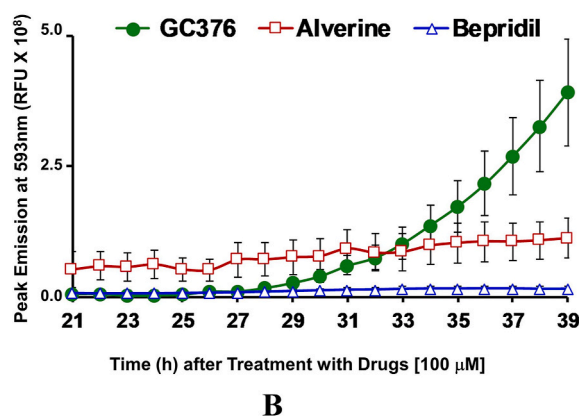
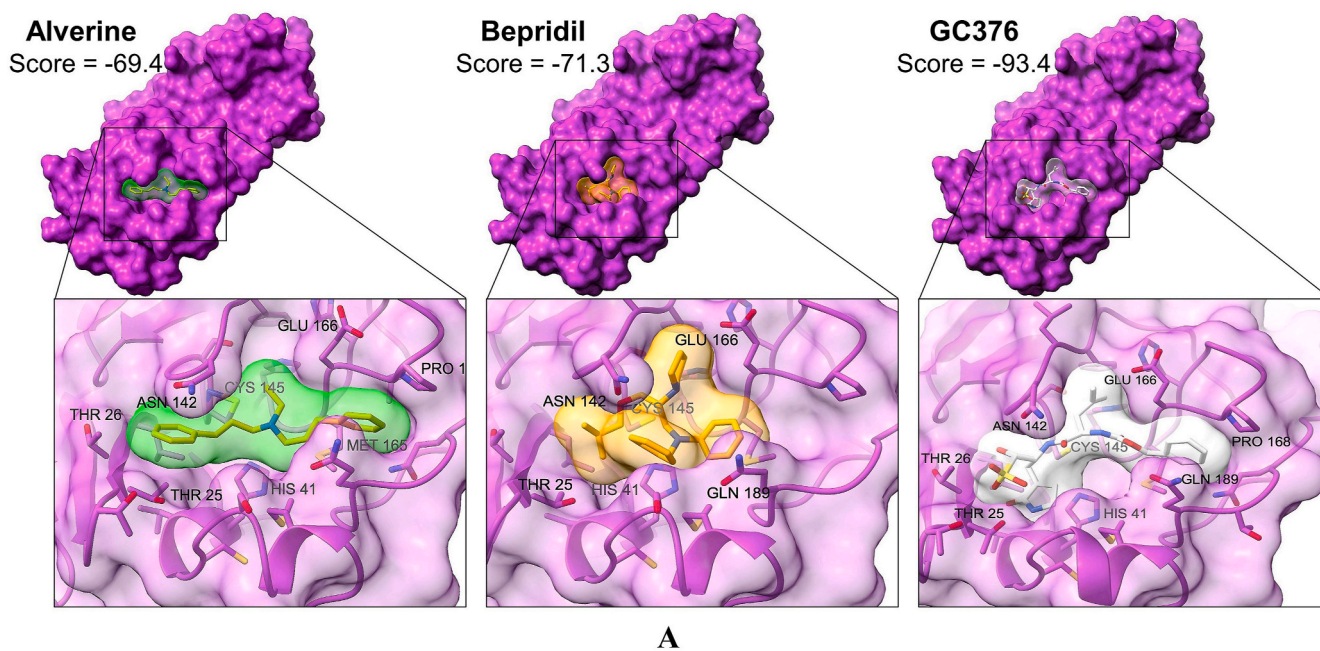


**Fig. 6.** Alverine and Bepridil are not effective intracellular inhibitors of CoV2 Mpro: A) The hierarchical fragment-based docking with dynamics protocol (CANDOCK) (Fine et al., 2020) was used to determine the predicted docking of two existing drugs (from the FDA approved drugs library) among those predicted to have the highest affinity to CoV2 Mpro (Mangione et al., 2020), Alverine and Bepridil, as well as GC376, onto one of the earliest deposited crystal structures of Mpro (pdb 6Y2e) (Zhang et al., 2020). The site on CoV2 Mpro that each drug was predicted to bind to was the catalytic pocket of CoV2 Mpro (Vatanev et al., 2021). The relative binding scores for each predicted interaction is presented, with Alverine showing the weaker of the predicted affinities (-69.4), Bepridil slightly higher affinity (-71.3), and GC376 having the highest predicted affinity (-93.4). B) to determine if Alverine or Bepridil demonstrated any appreciable inhibition of intracellular CoV2 Mpro, each drug was compared to GC376 for the ability to inhibit CoV2 Mpro activity at 100  $\mu\text{M}$  levels over time as in Fig. 4A, evaluating fluorescence each hour for 18 h following addition of 100  $\mu\text{M}$  of GC376 (circles), Alverine (squares), or Bepridil (triangles). Photomicrographs of cells treated with Alverine, Bepridil and also Ebselen, are shown in Supplemental Fig. 5A.

et al., 2021; Milligan et al., 2021; Brown et al., 2020), was not an effective inhibitor of CoV2 Mpro intracellularly by either fluorescence or RFP-AVLQS cleavage (Supplemental Fig. 5A and B).

### 3.7. Use of the cell-based CoV2 Mpro biosensor assay in evaluating recovery from Mpro inhibition

The viability of cells expressing these recombinant proteins and treated with GC376 allows for evaluation of recovery of intracellular Mpro activity following removal of the competitive inhibitor. If media containing Mpro-inhibiting GC376 is removed and replaced by fresh media; GC376 concentrations fall, the drug is no longer stably associated with Mpro (Vuong et al., 2020), and Mpro becomes capable of cleaving the RFP biosensor resulting in disappearance of RFP fluorescence.

CoV2 Mpro recovery was evaluated by treating RFP-AVLQS- and

Mpro-expressing cells with GC376 for 17 h, and then exchanging the drug-containing media for non-drug-containing media for 23 h and evaluating the loss of fluorescence due to Mpro becoming active. Inhibition of Mpro by GC376 for the 17 h treatment is readily seen for 1, 10 and 100  $\mu\text{M}$  levels (Fig. 7A solid bars), as shown above (Figs. 4 and 5), and 23 h after drug removal substantial decreases in fluorescence are seen (Fig. 7A hatched bars), while the cells remain viable (Fig. 7A triangles). (The cultures treated with 100  $\mu\text{M}$  GC376 retained fairly high RFP signal. This is likely due to levels of GC376 sufficient for Mpro inhibition remaining in the wells after media exchange. The wells were not rinsed to remove residual drug to prevent dislodging the cultured cell layer.) To evaluate the time-dependence of this recovery GC376 was used at 10  $\mu\text{M}$  and fluorescence was quantified at every hour during both drug treatment as well as after removal. Following removal of the GC376, fluorescence levels decreased over the first 2–3 h (Fig. 7B). Loss

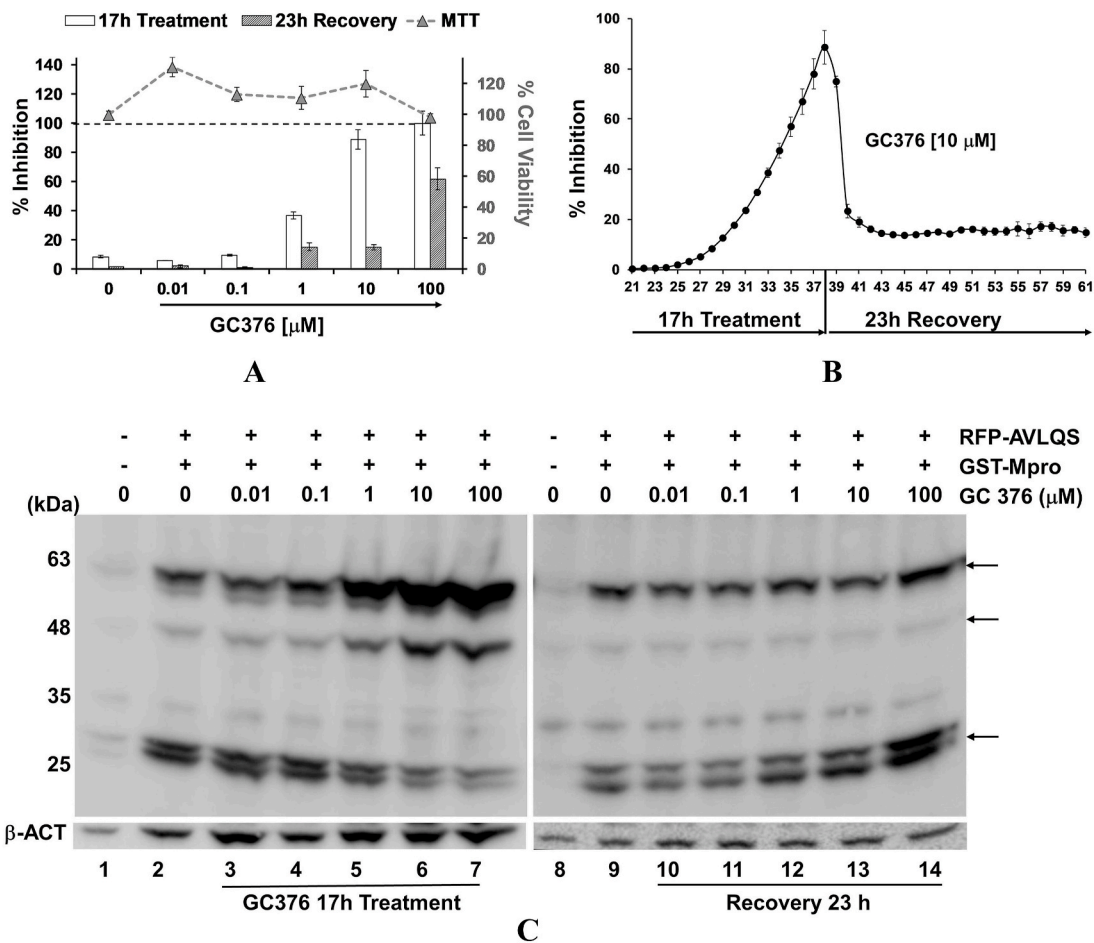


**Fig. 7.** Recovery of Mpro activity upon removal of GC376: We noted that GC376-treated cells retain excellent viability, allowing for removal of the drug-containing media, recovery of Mpro activity and loss of fluorescence. AD293 cells were transfected with both expression plasmids and treated with the indicated levels of GC376 for 17 h and fluorescence was evaluated every hour as in Fig. 4A. GC376-containing media was removed, replaced with OPTI-MEM, and plates returned to the imaging chamber and monitored hourly for another 23 h. A) Percentage inhibition of fluorescence due to CoV2 Mpro function was determined at the 17th hr following addition of drug (open bars) and at the 23rd hr after drug removal (hatched bars), setting treatment with 100  $\mu\text{M}$  GC376 at the 17th hr as 100% inhibition. Cell viability was plotted on the secondary axis as determined by MTT assay at the 23 h of recovery. Percentage viability (triangles) was calculated for each concentration setting no drug as 100% cell viability). B) The time dependence of Mpro recovery from GC376 was carried out with 10  $\mu\text{M}$  GC376, which provides outstanding Mpro inhibition (gain of fluorescence) and recovery (loss of fluorescence), while minimizing the effect of residual drug affecting Mpro function after drug removal (Fig. 7A). Percent inhibition (y axis) was determined throughout the 17 h of GC376 treatment, followed by 23 h of recovery after drug removal. C) Extracts from AD293 cells in 7A were immunoblotted for RFP after the 17 h drug treatment (left panels) and after the 23 h of recovery after removal of GC376 (right panels). Beta actin verified consistent levels of extract for each lane (lower panels). Immunoblotting for GST and GST-Mpro for these cultures provided in Supplemental Fig. 6 are consistent with the cleavage results for RFP (Fig. 7C).

of fluorescence corresponds to loss of the RFP 54 kDa protein (Fig. 7C). After 17 h treatment with 0.01–100  $\mu\text{M}$  GC376 (Fig. 7C, left upper panel) there was a dose-dependent increase in levels of the RFP 54 kDa protein, showing accumulation of the uncleaved RFP fluorescent polypeptide (consistent with increased fluorescence levels in these cultures, Fig. 7A), and a concomitant decrease in levels of the non-fluorescent 27 kDa cleaved RFP doublet. This demonstrated the inhibitory action of the drug on RFP cleavage by Mpro. Following the recovery period, the previously accumulated levels of 54 kDa RFP decreased to similar levels in extracts from all transfected cultures (right upper panel), consistent with loss of fluorescence (Fig. 7A). The cleavage of the previously accumulated 54 kDa was also evident by increased levels of the 27 kDa Mpro-cleaved polypeptides in extracts from cells previously treated with the higher levels of GC376. These conclusions were consistent with loss of the “drug-protected” GST-3CL fusion protein (in 10 and 100  $\mu\text{M}$  treated cultures) following drug removal (Supplemental Fig. 6), consistent with previous reports that GC376 inhibition of CoV2 Mpro is reversible (Vuong et al., 2020; Arutyunova et al., 2021).

#### 4. Discussion

The likelihood of CoV2 becoming endemic and novel zoonotic coronaviruses arising emphasize the need for antivirals effective against CoV2 and coronaviruses in general, leading to the recent US commitment to invest \$3.2 billion for development of antivirals (<https://www.cidrap.umn.edu>, 2021). Drugs that alter host cell pathways and/or immune function have been repurposed for use during the COVID-19 pandemic and have been helpful in saving lives during this crisis (RECOVERY Collaborative Group et al., 2021; Johnson and Vinetz, 2020; Maskin et al., 2020; Prescott and Rice, 2020; Villar et al., 2020); however, very few antivirals that attack CoV2 directly have been authorized for human use. The only antivirals currently available for use against COVID-19 are two RdRp inhibitors originally developed for other viruses, remdesivir and favipiravir (favipiravir has been approved for use in some Asian countries, but not in the US) (Costanzo et al., 2020; Service, 2021; McKee et al., 2020; Choy et al., 2020). More highly effective drugs developed for use against CoV2 and other CoVs are desperately needed for treatment of currently circulating CoV2 strains, or newly

arising strains that may be vaccine resistant (McCallum et al., 2021), as well as novel CoVs that may arise in the future.

It has been noted that RdRps and viral proteases are both excellent targets for CoV antivirals (Ali et al., 2020; Dong et al., 2021; Giovane et al., 2020; McKee et al., 2020). Indeed, for other viruses that require both a viral polymerase and a protease to cleave viral polyproteins, combinations of a protease inhibitor and a viral polymerase inhibitor have proven to be highly effective drug combinations (Kausar et al., 2021; Steuber and Hilgenfeld, 2010; Tompa et al., 2021; Kim et al., 2012). In addition to the repurposed RdRp inhibitor, remdesivir, there is a new CoV2 RdRp inhibitor, Molnupiravir (MK4482), and a CoV2 Mpro inhibitor, PF07321332, that are in early-stage clinical trials (<https://clinicaltrials.gov>, 2133; <https://clinicaltrials.gov>). Clearly, more than a single drug will be required for each of these targets, particularly given the rate at which coronavirus variants arise, as the use of antiviral drugs will select for viral mutants with decreasing sensitivity to existing drugs. The goal of our research was to develop a cell-based biosensor reporter assay to allow evaluation of CoV2 Mpro function inside living human cells that would not require biosafety level 3 containment. Many drugs and compounds have been evaluated as potential inhibitors of CoV2 Mpro using computational prediction programs, and some of these have been tested for function against CoV2 Mpro, generally against purified CoV2 Mpro (Costanzo et al., 2020; Fu et al., 2020; Ma et al., 2020a, 2020b; Drayman et al., 2020; McKee et al., 2020; Vatanserver et al., 2020; Zhu et al., 2020; Mangione et al., 2020; Brown et al., 2020; Choy et al., 2020; Shen et al., 2019), but this does not ensure that the drug will be effective intracellularly (Martinez, 2021). For example, our finding that Ebselen was not effective in this intracellular assay may be due to issues related to the oxidative state of Ebselen within living cells (Milligan et al., 2021). A small number of cell-based systems have been developed to evaluate CoV2 Mpro function, including assays based on loss of proliferation or luciferase expression, or based on HIV Tat-based transcription (Drayman et al., 2020; O'Brien et al., 2021; Rawson et al., 2021; Resnick et al., 2020). These approaches have limitations, as they result in cell death and/or require harvesting for evaluation of luciferase activity. Using a fluorescence readout allows one to evaluate activity without harvesting the cells. The flexibility of this type of assay is explicitly demonstrated when after 17 h of treatment with the effective Mpro inhibitor, GC376, the drug was removed and within 2 h the Mpro rapidly eliminated the accumulated RFP and any newly expressed RFP, resulting in loss of the fluorescent signal (Fig. 7A). This bodes well for adapting this system to a stable cell line that could be easily utilized to screen large libraries of compounds meeting high throughput challenges. A green fluorescent protein (GFP)-based CoV2 Mpro assay was developed based on Mpro cleavage and resultant re-localization of an HIV Tat-GFP construct, which provides for less-than-facile screening (Moghadasian et al., 2020). Also, a GFP-based CoV2 Mpro assay has been reported which functions in the reverse direction from the RFP system described herein – Mpro cleavage of their recombinant GFP protein allows the two GFP domains to associate and to produce green fluorescence signal (Froggatt et al., 2020). This GFP system does exhibit some of the advantages we describe above for the RFP system. However, when using these systems for high-throughput screening, the RFP system we describe here is superior to the GFP system because in this RFP system we use fully wild-type Mpro and because inhibition of Mpro function results in gain-of-signal rather than a loss-of-signal. A gain-of-signal produced by viral enzyme inhibition during drug screening provides an inherent internal counter-screen for cell viability, as well as for transcription and translation of new proteins. This will be of particular value when screening large collections of novel compounds, when unknown toxicity could inhibit GFP signal just as effectively as an Mpro inhibitor, leading to a necessity for subsequent screening steps. Mpro inhibition being screened by the appearance of RFP signal would eliminate the false positives caused by toxic compounds in the GFP screen. For these and other reasons, positive gain-of-signal provides screening inherently superior to loss-of-signal. In addition, unlike all other

reported cell-based CoV Mpro systems, the Mpro expressed in this system is wild-type CoV2 Mpro, producing a fully mature version that is self-cleaved to generate the native N-terminus beginning with the N-terminal serine residue. Using the fully native mature CoV2 Mpro will provide more accurate inhibitory determinations than evaluating inhibitor effects on a CoV2 Mpro with a non-native N-terminus, which is known to compromise Mpro activity (Xue et al., 2007). It is anticipated that this system will not only prove highly useful as a screening system for inhibitors of CoV2 Mpro, but will be readily adaptable to other CoV Mpro enzymes, as well as other viral and even cellular proteases. This system can also be utilized for analyzing protease function intracellularly, either of mutations within CoV2 Mpro, or of mutations in Mpro cleavage sites.

## Author contributions

TM and RDR designed the study; RDR carried out the transfections, microscopy, immunoblots, drug inhibition, cytotoxicity assays, and all data analyses; GRS designed, validated and prepared all plasmids; UT and SS designed, performed, and analyzed the SARS-CoV-2 infection experiments; ZF and RS designed and carried out the drug predictions and the drug docking onto the Mpro structure; TM and RDR wrote the manuscript. All authors had input into the final document and have given approval for the final version of the manuscript.

## Funding

This work was funded in part through support from NIH grant AI 128421 (to TM), in part through a SUNY Research Foundation COVID research seed grant award (RFP#20-03-COVID) (to TM, RDR and ZF), in part through contributions by the JSMBS and the Department of Microbiology & Immunology, and in part through generous contributions by donors to the UB Foundation's Papillomavirus Research Fund.

## Declaration of competing interest

The authors declare that they have no known competing financial interests or personal relationships that could have appeared to influence the work reported in this paper.

## Acknowledgment

We thank: Dr. Spencer Alford for advice on utilizing ddRFP, Dr. Patricia C. Weber for advice on viral protease screening, Dr. Jacques Archambault for helpful discussions on designing cell-based screening systems, Dr. Wade Sigurdson for assistance with microscopy and the Bio-Tek Cytation 1, and Dr. David Bruyette and Anivive Lifesciences for providing GC-376.

## Appendix A. Supplementary data

Supplementary data to this article can be found online at <https://doi.org/10.1016/j.antiviral.2021.105183>.

## References

- Alford, S.C., Abdelfattah, A.S., Ding, Y., Campbell, R.E., 2012. A fluorogenic red fluorescent protein heterodimer. *Chem. Biol.* 19, 353–360.
- Ali, M.J., Hanif, M., Haider, M.A., Ahmed, M.U., Sundas, F., Hirani, A., Khan, I.A., Anis, K., Karim, A.H., 2020. Treatment options for COVID-19: a review. *Front. Med.* 7, 480.
- Archambault, J., Melendy, T., 2013. Targeting human papillomavirus genome replication for antiviral drug discovery. *Antivir. Ther.* 18, 271–283.
- Arutyunova, E., Khan, M.B., Fischer, C., Lu, J., Lamer, T., Vuong, W., van Belkum, M.J., McKay, R.T., Tyrrell, D.L., Vederas, J.C., et al., 2021. N-terminal finger stabilizes the S1 pocket for the reversible feline drug GC376 in the SARS-CoV-2 M(pro) dimer. *J. Mol. Biol.* 433, 167003.
- Bhopal, R.S., 2020. COVID-19 zuzwang: potential public health moves towards population (herd) immunity. *Publ. Health Pract. (Oxf)* 1, 100031.

- Bobrowski, T., Chen, L., Eastman, R.T., Itkin, Z., Shinn, P., Chen, C.Z., Guo, H., Zheng, W., Michael, S., Simeonov, A., et al., 2021. Synergistic and antagonistic drug combinations against SARS-CoV-2. *Mol. Ther.* 29, 873–885.
- Brown, A.S., Ackerley, D.F., Calcott, M.J., 2020. High-throughput screening for inhibitors of the SARS-CoV-2 protease using a FRET-biosensor. *Molecules* 25.
- Cao, W.C., Liu, W., Zhang, P.H., Zhang, F., Richardus, J.H., 2007. Disappearance of antibodies to SARS-associated coronavirus after recovery. *N. Engl. J. Med.* 357, 1162–1163.
- Chopra, G., Kaushik, S., Elkin, P.L., Samudrala, R., 2016. Combating ebola with repurposed therapeutics using the CANDO platform. *Molecules* 21.
- Choy, K.T., Wong, A.Y., Kaewpreedee, P., Sia, S.F., Chen, D., Hui, K.P.Y., Chu, D.K.W., Chan, M.C.W., Cheung, P.P., Huang, X., et al., 2020. Remdesivir, lopinavir, emetine, and homoharringtonine inhibit SARS-CoV-2 replication in vitro. *Antivir. Res.* 178, 104786.
- Chuck, C.P., Chong, L.T., Chen, C., Chow, H.F., Wan, D.C., Wong, K.B., 2010. Profiling of substrate specificity of SARS-CoV 3CL. *PLoS One* 5, e13197.
- Costanzo, M., De Giglio, M.A.R., Roviello, G.N., 2020. SARS-CoV-2: recent reports on antiviral therapies based on lopinavir/ritonavir, darunavir/umifenovir, hydroxychloroquine, remdesivir, favipiravir and other drugs for the treatment of the new coronavirus. *Curr. Med. Chem.* 27, 4536–4541.
- Crooks, G.E., Hon, G., Chandonia, J.M., Brenner, S.E., 2004. WebLogo: a sequence logo generator. *Genome Res.* 14, 1188–1190.
- de Vries, M., Mohamed, A.S., Prescott, R.A., Valero-Jimenez, A.M., Desvignes, L., O'Connor, R., Steppan, C., Anderson, A.S., Binder, J., Dittmann, M., 2020. Comparative study of a 3CL (pro) inhibitor and remdesivir against both major SARS-CoV-2 clades in human airway models. *bioRxiv*.
- Debing, Y., Neyts, J., Delang, L., 2015. The future of antivirals: broad-spectrum inhibitors. *Curr. Opin. Infect. Dis.* 28, 596–602.
- Dong, Y., Shamsuddin, A., Campbell, H., Theodoratou, E., 2021. Current COVID-19 treatments: rapid review of the literature. *J. Glob. Health* 11, 10003.
- Drayman, N., Jones, K.A., Azizi, S.A., Froggatt, H.M., Tan, K., Maltseva, N.I., Chen, S., Nicolaescu, V., Dvorkin, S., Furlong, K., et al., 2020. Drug Repurposing Screen Identifies Masitinib as a 3CLpro Inhibitor that Blocks Replication of SARS-CoV-2 in Vitro (bioRxiv).
- Durante-Mangoni, E., Andini, R., Bertolino, L., Mele, F., Florio, L.L., Murino, P., Corcione, A., Zampino, R., 2020. Early experience with remdesivir in SARS-CoV-2 pneumonia. *Infection* 48, 779–782.
- Fine, J., Konc, J., Samudrala, R., Chopra, G., 2020. CANDOCK: chemical atomic network-based hierarchical flexible docking algorithm using generalized statistical potentials. *J. Chem. Inf. Model.* 60, 1509–1527.
- Froggatt, H.M., Heaton, B.E., Heaton, N.S., 2020. Development of a fluorescence-based, high-throughput SARS-CoV-2 3CL(pro) reporter assay. *J. Virol.* 94.
- Fu, L., Ye, F., Feng, Y., Yu, F., Wang, Q., Wu, Y., Zhao, C., Sun, H., Huang, B., Niu, P., et al., 2020. Both Boceprevir and GC376 efficaciously inhibit SARS-CoV-2 by targeting its main protease. *Nat. Commun.* 11, 4417.
- Giovane, R.A., Rezaei, S., Cleland, E., Henderson, C.E., 2020. Current pharmacological modalities for management of novel coronavirus disease 2019 (COVID-19) and the rationale for their utilization: a review. *Rev. Med. Virol.* 30, e2136.
- Graham, R.L., Baric, R.S., 2010. Recombination, reservoirs, and the modular spike: mechanisms of coronavirus cross-species transmission. *J. Virol.* 84, 3134–3146.
- Haseltine, W.A., 2020. <https://www.nbcnews.com/news/world/u-s-scientist-warns-coronavirus-vaccine-not-guaranteed-worldwide-cases-n1211826>. <https://clinicaltrials.gov/ct2/results?cond=&term=MK4482&cntry=&state=&city=&dist=> <https://clinicaltrials.gov/ct2/show/NCT04756531?term=PF07321332&draw=2&rank=2>. <https://www.aatbio.com/tools/ec50-calculator>. <https://www.cidrap.umn.edu/news-perspective/2021/06/white-house-announces-32-billion-toward-antivirals>.
- Hu, Y., Ma, C., Szeto, T., Hurst, B., Tarbet, B., Wang, J., 2021. Boceprevir, calpain inhibitors II and XII, and GC-376 have broad-spectrum antiviral activity against coronaviruses. *ACS Infect. Dis.* 7, 586–597.
- Jin, Z., Du, X., Xu, Y., Deng, Y., Liu, M., Zhao, Y., Zhang, B., Li, X., Zhang, L., Peng, C., et al., 2020. Structure of M(pro) from SARS-CoV-2 and discovery of its inhibitors. *Nature* 582, 289–293.
- Johnson, R.M., Vinetz, J.M., 2020. Dexamethasone in the management of covid-19. *BMJ* 370, m2648.
- Kalil, A.C., Patterson, T.F., Mehta, A.K., Tomashek, K.M., Wolfe, C.R., Ghazaryan, V., Marconi, V.C., Ruiz-Palacios, G.M., Hsieh, L., Kline, S., et al., 2021. Baricitinib plus remdesivir for hospitalized adults with covid-19. *N. Engl. J. Med.* 384, 795–807.
- Kausar, S., Said Khan, F., Ishaq Majeed Ur Rehman, M., Akram, M., Riaz, M., Rasool, G., Hamid Khan, A., Saleem, I., Shamim, S., Malik, A., 2021. A review: mechanism of action of antiviral drugs. *Int. J. Immunopathol. Pharmacol.* 35, 20587384211002621.
- Kim, Y., Lovell, S., Tiew, K.C., Mandadapu, S.R., Alliston, K.R., Battaile, K.P., Groutas, W. C., Chang, K.O., 2012. Broad-spectrum antivirals against 3C or 3C-like proteases of picornaviruses, noroviruses, and coronaviruses. *J. Virol.* 86, 11754–11762.
- Li, Q., Kang, C., 2020. Progress in developing inhibitors of SARS-CoV-2 3C-like protease. *Microorganisms* 8.
- Li, X., Giorgi, E.E., Marichannegowda, M.H., Foley, B., Xiao, C., Kong, X.P., Chen, Y., Gnanakaran, S., Korber, B., Gao, F., 2020. Emergence of SARS-CoV-2 through recombination and strong purifying selection. *Sci. Adv.* 6.
- Lin, Q., Zhu, L., Ni, Z., Meng, H., You, L., 2020. Duration of serum neutralizing antibodies for SARS-CoV-2: lessons from SARS-CoV infection. *J. Microbiol. Immunol. Infect.* 53, 821–822.
- Long, Q.X., Tang, X.J., Shi, Q.L., Li, Q., Deng, H.J., Yuan, J., Hu, J.L., Xu, W., Zhang, Y., Lv, F.J., et al., 2020. Clinical and immunological assessment of asymptomatic SARS-CoV-2 infections. *Nat. Med.* 26, 1200–1204.
- Ma, C., Sacco, M.D., Hurst, B., Townsend, J.A., Hu, Y., Szeto, T., Zhang, X., Tarbet, B., Marty, M.T., Chen, Y., et al., 2020a. Boceprevir, GC-376, and calpain inhibitors II, XII inhibit SARS-CoV-2 viral replication by targeting the viral main protease. *Cell Res.* 30, 678–692.
- Ma, C., Hu, Y., Townsend, J.A., Lagarias, P.L., Marty, M.T., Kolocouris, A., Wang, J., 2020b. Ebselen, Disulfiram, Carmofur, PX-12, Tideglusib, and Shikonin Are Non-specific Promiscuous SARS-CoV-2 Main Protease Inhibitors. *bioRxiv*.
- Mangione, W., Falls, Z., Melendy, T., Chopra, G., Samudrala, R., 2020. Shotgun drug repurposing biotechnology to tackle epidemics and pandemics. *Drug Discov. Today* 25, 1126–1128.
- Martinez, M.A., 2021. Lack of effectiveness of repurposed drugs for COVID-19 treatment. *Front. Immunol.* 12, 635371.
- Maskin, L.P., Olarte, G.L., Palizas Jr., F., Velo, A.E., Lurbet, M.F., Bonelli, I., Baredes, N. D., Rodriguez, P.O., 2020. High dose dexamethasone treatment for Acute Respiratory Distress Syndrome secondary to COVID-19: a structured summary of a study protocol for a randomised controlled trial. *Trials* 21, 743.
- McCallum, M., Bassi, J., De Marco, A., Chen, A., Walls, A.C., Di Iulio, J., Tortorici, M.A., Navarro, M.J., Silacci-Fregni, C., Saliba, C., et al., 2021. SARS-CoV-2 immune evasion by the B.1.427/B.1.429 variant of concern. *Science*.
- McKee, D.L., Sternberg, A., Stange, U., Laufer, S., Naujokat, C., 2020. Candidate drugs against SARS-CoV-2 and COVID-19. *Pharmacol. Res.* 157, 104859.
- Melgaco, J.G., Azamor, T., Ano Bom, A.P.D., 2020. Protective immunity after COVID-19 has been questioned: what can we do without SARS-CoV-2-IgG detection? *Cell. Immunol.* 353, 104114.
- Milligan, J.C., Zeisner, T.U., Papageorgiou, G., Joshi, D., Souly, C., Ulferts, R., Wu, M., Lim, C.T., Tan, K.W., Weissmann, F., et al., 2021. Identifying SARS-CoV-2 antiviral compounds by screening for small molecule inhibitors of Nsp5 main protease. *Biochem. J.* 478, 2499–2515.
- Mitchell, A.C., Alford, S.C., Hunter, S.A., Kannan, D., Parra Sperberg, R.A., Chang, C.H., Cochran, J.R., 2018. Development of a protease biosensor based on a dimerization-dependent red fluorescent protein. *ACS Chem. Biol.* 13, 66–72.
- Moghadas, S.A., Becker, J.T., Belica, C., Wick, C., Brown, W.L., Harris, R.S., 2020. Gain-of-function Assay for SARS-CoV-2 M (Pro) Inhibition in Living Cells. *bioRxiv*.
- Muramatsu, T., Takemoto, C., Kim, Y.T., Wang, H., Nishii, W., Terada, T., Shirouzu, M., Yokoyama, S., 2016. SARS-CoV 3CL protease cleaves its C-terminal autoproteolytic site by novel subsite cooperativity. *Proc. Natl. Acad. Sci. U. S. A.* 113, 12997–13002.
- Neerukonda, S.N., Katmeni, U., 2020. A review on SARS-CoV-2 virology, pathophysiology, animal models, and anti-viral interventions, 9. *Pathogens*.
- O'Brien, A., Chen, D.Y., Hackbart, M., Close, B.J., O'Brien, T.E., Saeed, M., Baker, S.C., 2021. Detecting SARS-CoV-2 3CLpro expression and activity using a polyclonal antiserum and a luciferase-based biosensor. *Viruology* 556, 73–78.
- Payne, D.C., Smith-Jeffcoat, S.E., Nowak, G., Chukwura, U., Geibe, J.R., Hawkins, R.J., Johnson, J.A., Thornburg, N.J., Schiffer, J., Weiner, Z., et al., 2020. SARS-CoV-2 infections and serologic responses from a sample of U.S. Navy Service members - USS Theodore Roosevelt, April 2020. *MMWR Morb. Mortal. Wkly. Rep.* 69, 714–721.
- Pillaiyar, T., Manickam, M., Namasivayam, V., Hayashi, Y., Jung, S.H., 2016. An overview of severe acute respiratory syndrome-coronavirus (SARS-CoV) 3CL protease inhibitors: peptidomimetics and small molecule chemotherapy. *J. Med. Chem.* 59, 6595–6628.
- Prescott, H.C., Rice, T.W., 2020. Corticosteroids in COVID-19 ARDS: evidence and hope during the pandemic. *J. Am. Med. Assoc.*
- Pruijssers, A.J., George, A.S., Schafer, A., Leist, S.R., Gralinski, L.E., Dinno 3rd, K.H., Yount, B.L., Agostini, M.L., Stevens, L.J., Chappell, J.D., et al., 2020. Remdesivir inhibits SARS-CoV-2 in human lung cells and chimeric SARS-CoV expressing the SARS-CoV-2 RNA polymerase in mice. *Cell Rep.* 32, 107940.
- Rathnayake, A.D., Zheng, J., Kim, Y., Perera, K.D., Mackin, S., Meyerholz, D.K., Kashipathy, M.M., Battaile, K.P., Lovell, S., Perlman, S., et al., 2020. 3C-like protease inhibitors block coronavirus replication in vitro and improve survival in MERS-CoV-infected mice. *Sci. Transl. Med.* 12.
- Rawson, J.M.O., Duchon, A., Nikolaitchik, O.A., Pathak, V.K., Hu, W.S., 2021. Development of a cell-based luciferase complementation assay for identification of SARS-CoV-2 3CL(pro) inhibitors. *Viruses* 13.
- RECOVERY Collaborative Group, Horby, P., Lim, W.S., Emberson, J.R., Mafham, M., Bell, J.L., Linsell, L., Staplin, N., Brightling, C., Ustianowski, A., et al., 2021. Dexamethasone in hospitalized patients with covid-19 - preliminary report. *N. Engl. J. Med.* 384 (8), 693–704. <https://doi.org/10.1056/NEJMoa2021436>.
- Resnick, S.J., Iketani, S., Hong, S.J., Zask, A., Liu, H., Kim, S., Melore, S., Nair, M.S., Huang, Y., Tay, N.E.S., et al., 2020. A Simplified Cell-Based Assay to Identify Coronavirus 3CL Protease Inhibitors. *bioRxiv*.
- Riss, T.L., Moravec, R.A., Niles, A.L., Duellman, S., Benink, H.A., Worzella, T.J., Minor, L., Markossian, S., Sittampalam, G.S., Grossman, A., et al., 2004. Cell Viability Assays. Eli Lilly & Company and the National Center for Advancing Translational Sciences, Bethesda (MD).
- Service, R.F., 2021. A call to arms. *Science* 371, 1092–1095.
- Shen, L., Niu, J., Wang, C., Huang, B., Wang, W., Zhu, N., Deng, Y., Wang, H., Ye, F., Cen, S., et al., 2019. High-throughput screening and identification of potent broad-spectrum inhibitors of coronaviruses. *J. Virol.* 93.
- Steuber, H., Hilgenfeld, R., 2010. Recent advances in targeting viral proteases for the discovery of novel antivirals. *Curr. Top. Med. Chem.* 10, 323–345.
- Sun, L.Y., Chen, C., Su, J., Li, J.Q., Jiang, Z., Gao, H., Chigan, J.Z., Ding, H.H., Zhai, L., Yang, K.W., 2021. Ebsulfur and Ebselen as highly potent scaffolds for the development of potential SARS-CoV-2 antivirals. *Bioorg. Chem.* 112, 104889.

- Tang, F., Quan, Y., Xin, Z.T., Wrammert, J., Ma, M.J., Lv, H., Wang, T.B., Yang, H., Richardus, J.H., Liu, W., et al., 2011. Lack of peripheral memory B cell responses in recovered patients with severe acute respiratory syndrome: a six-year follow-up study. *J. Immunol.* 186, 7264–7268.
- Tompa, D.R., Immanuel, A., Srikanth, S., Kadhivel, S., 2021. Trends and strategies to combat viral infections: a review on FDA approved antiviral drugs. *Int. J. Biol. Macromol.* 172, 524–541.
- Vatanever, E.C., Yang, K., Kratch, K.C., Drelich, A., Cho, C.C., Mellot, D.M., Xu, S., Tseng, C.K., Liu, W.R., 2020. Targeting the SARS-CoV-2 Main Protease to Repurpose Drugs for COVID-19. *bioRxiv*.
- Vatanever, E.C., Yang, K.S., Drelich, A.K., Kratch, K.C., Cho, C.C., Kempaiah, K.R., Hsu, J.C., Mellott, D.M., Xu, S., Tseng, C.K., et al., 2021. Bepridil is potent against SARS-CoV-2 in vitro, 118. *Proc Natl Acad Sci U S A*.
- Villa, T.G., Feijoo-Siota, L., Rama, J.L.R., Ageitos, J.M., 2017. Antivirals against animal viruses. *Biochem. Pharmacol.* 133, 97–116.
- Villar, J., Anon, J.M., Ferrando, C., Aguilar, G., Munoz, T., Ferreres, J., Ambros, A., Aldecoa, C., Suarez-Sipmann, F., Thorpe, K.E., et al., 2020. Efficacy of dexamethasone treatment for patients with the acute respiratory distress syndrome caused by COVID-19: study protocol for a randomized controlled superiority trial. *Trials* 21, 717.
- Vuong, W., Khan, M.B., Fischer, C., Arutyunova, E., Lamer, T., Shields, J., Saffran, H.A., McKay, R.T., van Belkum, M.J., Joyce, M.A., et al., 2020. Feline coronavirus drug inhibits the main protease of SARS-CoV-2 and blocks virus replication. *Nat. Commun.* 11, 4282.
- Williamson, B.N., Feldmann, F., Schwarz, B., Meade-White, K., Porter, D.P., Schulz, J., van Doremalen, N., Leighton, I., Yinda, C.K., Perez-Perez, L., et al., 2020. Clinical benefit of remdesivir in rhesus macaques infected with SARS-CoV-2. *Nature* 585, 273–276.
- Wu, L.P., Wang, N.C., Chang, Y.H., Tian, X.Y., Na, D.Y., Zhang, L.Y., Zheng, L., Lan, T., Wang, L.F., Liang, G.D., 2007. Duration of antibody responses after severe acute respiratory syndrome. *Emerg. Infect. Dis.* 13, 1562–1564.
- Wu, A., Wang, Y., Zeng, C., Huang, X., Xu, S., Su, C., Wang, M., Chen, Y., Guo, D., 2015. Prediction and biochemical analysis of putative cleavage sites of the 3C-like protease of Middle East respiratory syndrome coronavirus. *Virus Res.* 208, 56–65.
- Xue, X., Yang, H., Shen, W., Zhao, Q., Li, J., Yang, K., Chen, C., Jin, Y., Bartlam, M., Rao, Z., 2007. Production of authentic SARS-CoV M(pro) with enhanced activity: application as a novel tag-cleavage endopeptidase for protein overproduction. *J. Mol. Biol.* 366, 965–975.
- Zhang, L., Lin, D., Sun, X., Curth, U., Drosten, C., Sauerhering, L., Becker, S., Rox, K., Hilgenfeld, R., 2020. Crystal structure of SARS-CoV-2 main protease provides a basis for design of improved alpha-ketoamide inhibitors. *Science* 368, 409–412.
- Zhu, W., Xu, M., Chen, C.Z., Guo, H., Shen, M., Hu, X., Shinn, P., Klumpp-Thomas, C., Michael, S.G., Zheng, W., 2020. Identification of SARS-CoV-2 3CL Protease Inhibitors by a Quantitative High-Throughput Screening. *bioRxiv*.